CISTER
Research Centre in
Real-Time & Embedded
Computing Systems

Journal Paper

MIRAU-Net :An Improved Neural Network Based on U-Net for Gliomas Segmentation

Nagwa M. Aboelenein
Piao Songhao
Alam Noor*
Pir Noman Ahmad

*CISTER Research Centre

CISTER-TR-211102

2021

MIRAU-Net :An Improved Neural Network Based on U-Net for Gliomas Segmentation

Nagwa M. Aboelenein, Piao Songhao, Alam Noor*, Pir Noman Ahmad

*CISTER Research Centre

Polytechnic Institute of Porto (ISEP P.Porto)

Rua Dr. António Bernardino de Almeida, 431

4200-072 Porto

Portugal

Tel.: +351.22.8340509, Fax: +351.22.8321159

E-mail: alamn@isep.ipp.pt

https://www.cister-labs.pt

Abstract

Gliomas are the largest prevalent and destructive of brain tumors and have crucial parts for the diagnosing and treating of MRI brain tumors during segmentation using computerized methods. Recently, U-Net architecture has achieved impressive brain tumor segmentation, but this role remains challenging due to the differing severity and appearance of gliomas. Therefore, we proposed a novel encoder-decoder architecture called Multi Inception Residual Attention U-Net (MIRAU-Net) in this work. It integrates residual, inception modules with attention gates into U-Net to further enhance brain tumor segmentation performance. Encoderdecoder is connected in this architecture through Inception Residual pathways to decrease the distance between their maps of features. We use the weight crossentropy and generalized Dice (GDL) with focal Tversky loss functions to resolve the class imbalance problem. The evaluation performance of MIRAU-Net checked with Brats 2019 and obtained mean dice similarities of 0.885 for the whole tumor, 0.879 for the core area, and 0.818 for the enhancement tumor. Experiment results reveal that the suggested MIRAU-Net beats its baselines and provides better efficiency than recent techniques for brain tumor segmentation.

MIRAU-Net :An Improved Neural Network Based on U-Net for Gliomas Segmentation

Nagwa M. AboElenein[1,2], Piao Songhao[1], Alam Noor[3], Pir Noman Ahmed[1]

Harbin Institute of Technology, Harbin 150001, China

Abstract

Gliomas are the largest prevalent and destructive of brain tumors and have crucial parts for the diagnosing and treating of MRI brain tumors during segmentation using computerized methods. Recently, U-Net architecture has achieved impressive achievement in brain tumor segmentation, but this role remains challenging due to the differing severity and appearance of gliomas. Therefore, in this work, we proposed a novel encoder-decoder architecture called Multi Inception Residual Attention U-Net (MIRAU-Net). It integrates residual inception modules with attention gates into U-Net to further enhance brain tumor segmentation performance. Encoder-decoder is both connected in this architecture through Inception Residual pathways to decrease the distance between their maps of features. We use the weight cross-entropy and generalized Dice (GDL) with focal Tversky loss functions to resolve the class imbalance problem. The evaluation performance of MIRAU-Net checked with Brats 2019 and obtained mean dice similarities of 0.885 for the whole tumor, 0.879 for the core area, and 0.818 for the enhancement tumor. Experiment results reveal that the suggested MIRAU-Net beats its baselines and provides better efficiency than recent techniques for brain tumor segmentation.

Keywords: `Brain Tumor Segmentation`, U-Net, full convolutional network,

*Corresponding author

Email address: `piaosh@hit.edu.cn` (Piao Songhao)

[1]Harbin Institute of Technology, Harbin 150001, China

[2]Faculty of Computers and Information, Menoufia University,Shebin El-koom 32511, Egypt

[3]CISTER Research Centre, ISEP, Politécnico do Porto, Portugal

Inception, Residual Module, Attention Gate

1. Introduction

Gliomas are the most prominent brain tumors in adults caused by the glial cells [1]. The average occurrence of gliomas is about 190k annually worldwide [2]. It has two types with high-grade (HG) and low-grade (LG) glioma. HG glioma tumors are malignant and eventually grow and requiring surgery where the projected patient lifespan is two years or less and similarly a few years follow LG glioma (LGG) tumors. Magnetic resonance imaging (MRI) is a common non-invasive imaging technology that generates brain images of high quality without injury and artifacts from the skull for brain tumor screening and tracking. Gliomas are very difficult to recognize with handcrafted segmentation due to differences in brain tumor scale, shape, and function, but it is also time-intensive and tedious to segment manually. Automated segmentation can lead to a more accurate and more straightforward diagnosis and treatment. Automatic image segmentation approaches using deep learning methods [3] have recently made significant strides. Havaei et al.[4] applied multi-pathway CNNs into brain tumor segment regions. Also, two training steps were used to resolve the imbalanced input data class due to the size of image patches; however, their methods suffer from high computational cost and low performance. Shen et al.[5] built a boundary-aware a fully convolutional network (FCN) to improve tumor boundary and extracted from MRI scans contextual information with low computational efficiency. Based on this architecture, a fully convolutional network named U-Net was proposed by Ronneberger et al. [6] which implemented a completely convolutionary symmetrical network called U-Net for the segmentation of medical images. These networks are typically a down-sampling subnetwork that collects the high-level image functionality and an up-sampling subnet that reconstructs the pixel segmentation from these high-level features. However, at the beginning of the network, the contextual knowledge of the encoder function is inadequate, resulting in low output for the pixel identification

when paired with the corresponding high-grade decoder feature map. There are many variants of U-Net, such as combinations with modules like ResNet [7], DenseNet [8]. Integrating Inception modules in a U-Net architecture has also been recently proposed for brain tumor segmentation. Cahall et al. [9] introduced a new framework building on U-Net architecture and Inception module to segment glioma sub-regions and to segment intra-tumoral structures, which produced a positive impact only on the whole tumor while not affecting tumor core and enhancing tumor. While resolving such challenges, attention mechanisms have been shown to capture long-term dependencies and essential responses in computer vision. Many attempts to enhance image recognition and image segmentation efficiency have been carried out with the attention module. Wang et al. [10] create a residual attentiveness network that generates attention features from multiple modules, adjusting to deeper layers and enhancing classification accuracy effectively. Hu et al. [11] suggested a Squeeze and Excitation (SE) block attention module based on the channel relationship and dynamically recalibrating the function to improve feature expression. Zhang et al. [12] suggested AGResU-Net combines residual modules and attention gates with U-Net architecture. However, their methodology loses a significant quantity of background information and local details across different slices. It is noted that brain tumors have diverse shapes and sizes, which contribute to small tumors in the brain tumor segmentation. Taking into consideration the attention modules can increase the U-Net segmentation efficiency of small-scale tumors. We intend to explore the efficiency of an attention gate, efficient inception, and residual modules; for the brain tumor segmentation, we propose a novel Multi Inception Residual Attention U-Net model (MIRAU-Net). Experiments on brain tumor segmentation benchmark demonstrate that our MIRAU-Net can obtain comparable segmentation accuracy. This paper summarizes the major contributions as follows:

(1) We suggest an end-to-end MIRAU-Net model for the segmentation of the brain tumor.Figure 1 displays the MIRAU-Net architecture that extracts substantially more features to gain and restore information about the locations

of brain tumors, which enhances segmentation efficiency.

(2) MIRAU-Net combines Inception-residual modules and attention modules with U-Net architecture. Encoder and decoder sub-networks are linked in MIRAU-Net by Inception-Res paths to deeper and extend the proposed network. The re-modeled skip paths of the architecture with gate signal are forwarded to the attention gate attempt to Improve the capacity of expression and feature extraction and decrease the gap between the encoder and decoder sub-networks.

(3) A new multi-loss function is introduced, combining weight Loss, Generalized Dice Loss, and Focal Tversky Loss to mitigate the class imbalance.

(4) Experimental results on the Brats 2019 dataset for brain tumor segmentation illuminate that our model 2D Multi Inception Residual Attention U-Net (MIRAU-Net) is efficient and performs favorably against state-of-the-art methods.

Following this introduction, the detail of the suggested architecture is provided in Section 2. In Section 3, the experimental results and discussion are seen. In the end, Section 4 offers a conclusion and future work.

2. Methods

The detailed methodology of MIRAU-Net for brain tumor segmentation is given in this section. Then we provide a brief introduction to the multi-loss function adopted in MIRAU-Net.

2.1. Multi Inception-Residual Attention U-Net (MIRAU-Net)

The U-Net network is more capable of feature representation, so more contextual knowledge is collected based on the U-Net. A novel end-to-end fully connected network is proposed that incorporates the Inception-Res module with an attention gate unit into the U-Net module. Fig.1 illustrates the architecture of the proposed Multi Inception Residual Attention U-Net, known as MIRAU-Net.

We are deeper into the U-Net by replacing the sequence of two convolutional layers in both encoder and decoder layers in the original U-Net model with the proposed Inception-Res block; also, we introduce re-modeled skip pathways, namely Inception-Res skip connection. We provide adequate spatial information and the positioning of low-level feature maps using attention gates to increase segmentation accuracy for small-scale tumors during the up-sampling process.

2.1.1. Inception-Residual U-Net

The medical image objects have varying sizes. A network must also be able to identify entities on different scales to enhance segmentation efficiency. Szegedy [13] introduced the architecture of Inception-Res blocks, which using variable kernel size convolutionary layers to extract features from different image scales. We update the U-Net architecture with a modified Inception-Residual module to improve network representation functionality and segmentation efficiency. The modified Inception-Res module is proposed to be used in each block shown in Fig 2 includes multiple sets of 1×1 convolutions, 3×1 convolutions, and 1x3 convolutions. The output filters generated from the convolution layers in the first branch 1x1 concatenated with convolution layers in the second branch 1x1,1x3,3x1 then this output added with the convolution layers in the third branch 1x1. Compared with the original Inception–Res module first, Batch normalization (BN) layers after every convolutional layer in the architecture are added to prevent vanishing of gradient problems in MIRU-Net, which is adopted. Secondly, 1x1 convolutions applied on the identity feature map to preserve a similar relationship between the base U-Net number of filters and our suggested model, and PReLU activation [14] rather than ReLU activation in the baseline U-Net[6].

2.1.2. Re-designed skip Path

In the original U-Net, the encoder feature maps are received straight from the decoder. So in the MIRAU-Net, we made some modifications in skip connection called Inception-Res Path between encoder and decoder. Dataflow passes

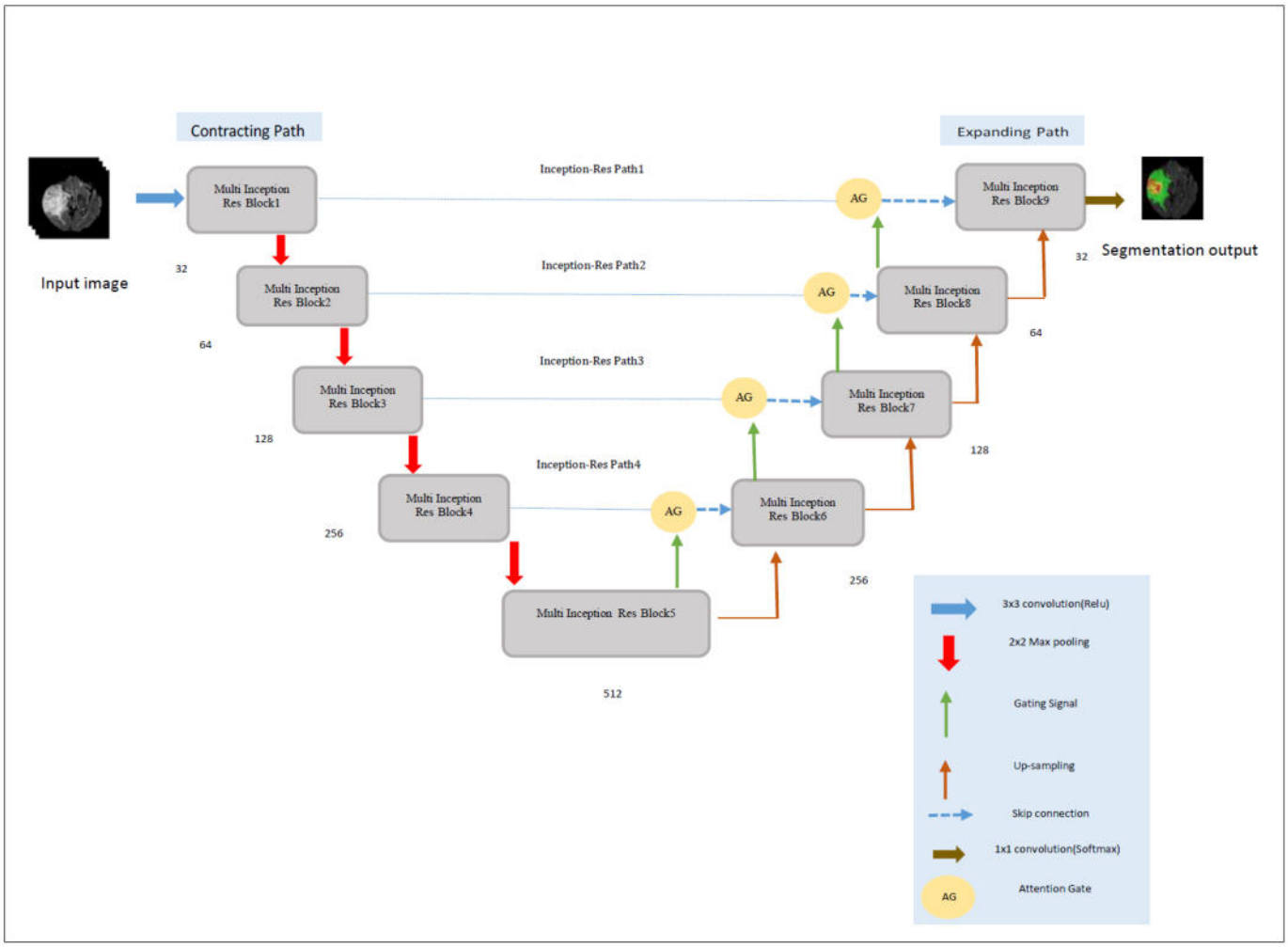

Figure 1: The architecture of the MIRAU-Net model.

through the chain of convolutional layers using inception residual connections methodology, concatenates with gating signal, and then forwards the output to the attention gate. The Inception-Res Path is illustrated in Fig. 3. We presumed the strength of the semantic distance between maps of the encoder and the decoder is likely to decrease. Therefore the convolutional blocks adopted

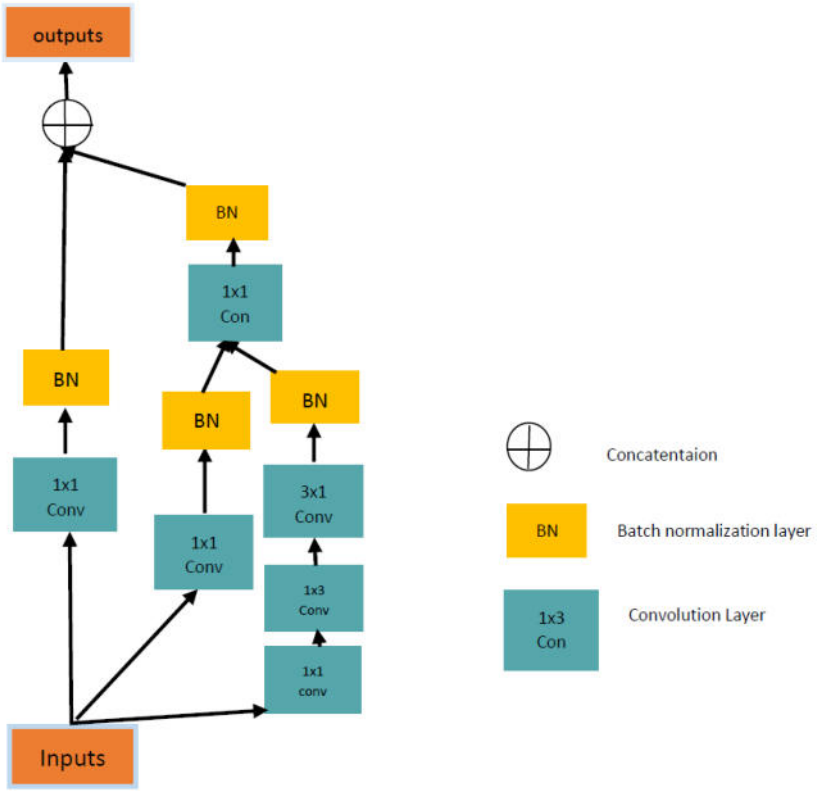

Figure 2: The modified Inception-Res module.

respectively along the four inception-Res paths. Besides the number of function maps in encoder-decoder, the blocks of the four Inception-Res paths comprise of multiple of 32 up to 256 filters, respectively. The details of Inception-Res paths are listed in Table 1.

2.1.3. Attention gate

Research has shown that a deep learning model that is trained with the attention gate increases network performance [10]. In Fig 4, attention gate device is illuminated and the output of AG x_{output} is an element-wise multiplication of input feature-maps x_l, and attention coefficients α. In this figure,x_l andg_i are Input feature map of layer l and gating signal, respectively the basic formula of

Table 1: Inception-Res paths details

Path	Layers	Number of filters
Inception-Res Path1	Conv2D(1,1)	32
	Conv2D(1,3)	32
	Conv2D(3,1)	32
	Conv2D(1,1)	32
	Conv2D(1,1)	32
Inception-Res Path2	Conv2D(1,1)	64
	Conv2D(1,3)	64
	Conv2D(3,1)	64
	Conv2D(1,1)	64
	Conv2D(1,1)	64
Inception-Res Path3	Conv2D(1,1)	128
	Conv2D(1,3)	128
	Conv2D(3,1)	128
	Conv2D(1,1)	128
	Conv2D(1,1)	128
Inception-Res Path4	Conv2D(1,1)	256
	Conv2D(1,3)	256
	Conv2D(3,1)	256
	Conv2D(1,1)	256
	Conv2D(1,1)	256

which is as follows:

$$x_{output} = x_l.\alpha_i \tag{1}$$

To obtain the gating coefficient we use additive attention [15]. Though computationally more costly, it has proved experimentally more efficient than multiplying attention .

$$\alpha_i = \sigma_2(\psi^T(\sigma_1(W_x^T x_l + W_g^T g_i + b_g)) + b_\psi) \tag{2}$$

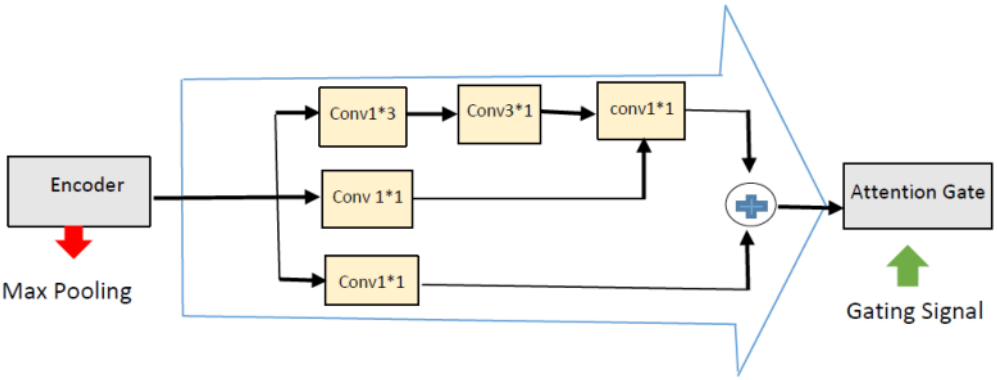

Figure 3: Inception-Res Path.

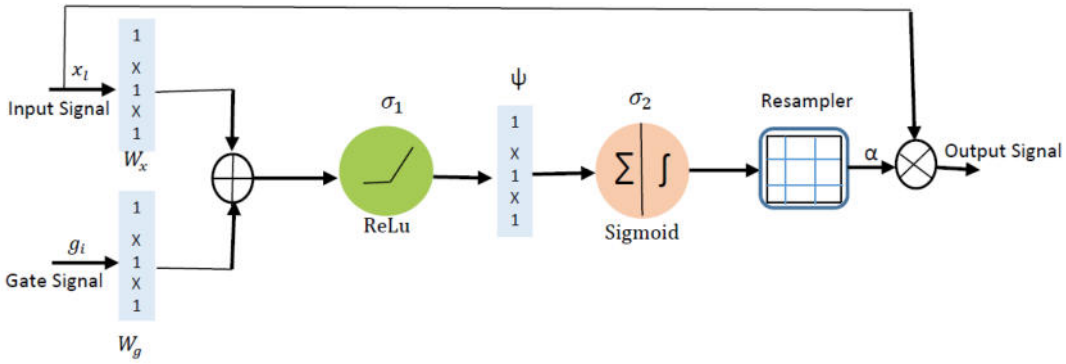

Figure 4: The basic block diagram of additive attention gate.

$\sigma_1$is sometimes selected as rectified linear function $\sigma_1(x_{l_{i,c}}) = max(0, x_{l_{i,c}})$where i and c represent spatially, and channel dimensions, respectively, and σ_2 corresponds to the Sigmoid activation function $\sigma_2(x_{l_{i,c}}) = \frac{1}{1+\exp(-x_{l_{i,c}})}$. W_x, $W_g$and ψ are linear transformations, while b_g and b_ψ are bias terms.

2.2. Multi Loss Function

The efficiency of the segmentation model depends on the loss function option, not only on the architecture of the network, especially when dealing with an extremely imbalanced problem. Therefore, it becomes more difficult to choose a suitable loss function. We utilize weight cross-entropy loss[16], a Generalized Dice loss (GDL)[17], and focal tversky loss[18] to fix unbalance label class. In this study, we utilize a multi loss function, defined in Equation (3):

$$MultiLoss = GDL + WCE + FocalTverskyLoss \tag{3}$$

2.2.1. Generalized Dice Loss (GDL):

Suggested in Equation (3) as a multi-class segmentation estimating method which deal with label unbalance for medical images data:

$$GDL = 1 - 2\frac{(\sum_{i}^{L} w_i \sum_{i} g_{i_k}\ p_{i_k})}{\sum_{i}^{L} w_i \sum_{i}(\ g_{i_k} +\ p_{i_k})} \tag{4}$$

Where L represents the total number of labels, k is the size of a batch, w_i is the weight of the label i^{th} label. As suggested in[17], we have defined $w_i = \frac{1}{\sum_k g_{i_k}}$. p_{i_k} and g_{i_k} which represent the value of the (i^{th}, k^{th}) pixel of the binary ground truth image and binary segmented image .

2.2.2. Weighted cross-entropy (WCE):

The cross-entropy loss is chosen for the segmentation task, that accelerates learning at the beginning of the training,as seen in Equation 4:

$$WCE = \frac{-1}{k}\sum k \sum_{i}^{L} W_i g_{ik} log(p_{ik}) \tag{5}$$

2.2.3. Focal Tversky Loss:

Tversky index (TI) is a Dices coefficient generalization. TI adds weight to FP (false positives) and FN (false negatives), it can be defined as follows:

$$TI = \frac{TP + \epsilon}{TP + \alpha FN + (1 - \alpha)FP + \epsilon} \tag{6}$$

$$FTL = (1 - TI)^{\gamma} \tag{7}$$

Where γ varies between 1, and 3. Theϵ provides numerical stability to avoid division by zero. In our experiments, we observe that the highest performance, when $\gamma = 1.3$,and α=0.7.

3. Experimental Results

In this section, we briefly explained data pre-processing and experimental results of the proposed MIRAU-Net with the comparison of the previous novel research work.

3.1. Datasets

In this study, Brats 2019 brain tumor MRI dataset used for the performance evaluation. The Brats 2019 dataset contains 335 patients, 259 HGG cases, and 76 cases of LGG. At the same time, 125 patients are present in the validation Brats 2019 dataset. Each case contains volumes of FLAIR, T1, T1, and T2. The dataset is co-registered, re-sampled, and skull stripped to 1 mm3. There are four corresponding regions on the label: healthy, necrosis and non-enhancing, edema, and enhancing tumor where the whole tumor (WT) region includes all intratumor regions, i.e., necrosis non-enhancing tumor, edema, and enhancing tumor, Tumor core (TC) region that incorporates non-enhancing tumor necrosis and enhancing tumor (ET) region.

3.2. Experiment Details

For pre-processing, each slice is normalized with the mean and standard deviation of this slice. 2D patches during the training of 128x128x4 are randomly sampled to minimize processing time. All experiments are performed using the Keras framework with the TensorFlow backend [19]. Parametric Rectified Linear Unit (PReLU) function is used as an activation function. For 30 epochs,

we trained the model because validation loss did not change afterward. Evaluation results of BraTS2019 training and validation datasets are disseminated on the challenge leaderboard Web site. Our final results can be found in the leaderboard section of these challenges under the heading "Attention Inception Residual".

3.3. Evaluation metrics

In this study, we adopt used Dice score [20] and Hausdorff Distance [21]for WT, ET, and TC for evaluation of the segmentation results in the MIRAU-Net model. The Dice similarity score measures the overlap rate between P1 and T1 as follows:

$$DSC(P1, T1) = \frac{2|P1 \cap T1|}{|P1| + |T1|} \tag{8}$$

Where P1 and T1 denote the output segmentation, and label of ground-truth, respectively. The Hausdorff distance between the two surfaces of A and B is shown in the following Eq.

$$HD(A, B) = max(h(A, B), h(B, A)) \tag{9}$$

$$h(A, B) = max_{a \in A}\{\min{}_{b \in B}\{d(a, b)\}\} \tag{10}$$

Where d(a,b) represents the Euclidean distance between a and b.

3.4. Experiment Results

3.4.1. Evaluation Results on BraTS2019 Training Dataset

We take in this experiment 184 samples from the Brats 2019 training dataset using 80 percent of this dataset (147 subjects) for training and the remaining 20 percent (37 subjects) validation. The evaluation results of the proposed MIRAU-Net on the Brats 2019 training dataset are presented in Table2. Quantitatively the proposed network achieves Dice scores of 0.885 for the whole tumor, 0.879 for core tumor, and 0.818 enhancing tumor. Also, the mean, standard deviation, median, and 25th and 75th percentile of each metric are shown in the table. The segmentation efficiency of our training dataset algorithm can

be evaluated by DSC, Hausdorff distance, which is measured using the online evaluation system on the leaderboard Brats 2019 online website[4]. Also, in Table 3 we compare our MIRAU-Net with other typical brain tumor segmentation approaches from the literature to evaluate its performance.

Table 2: Dice and Hausdorff measurements on Brats 2019 Training Dataset

	Dice			Hausdorff distance		
	Whole	Core	Enhancing	Whole	Core	Enhancing
Mean	0.888	0.876	0.819	7.02	7.2	5.2
Std.Dev.	0.083	0.124	0.164	12.11	14.96	12.5
Median	0.91	0.918	0.91	3.7	3	2
25 quantile	0.87	0.86	0.78	2.4	2	1.4
75quantile	0.938	0.94	0.90	6.3	5.04	3.16

Table 3: Comparison of segmentation results on the Brats 2019 Training Dataset with typical methods

Methods	DSC			Hausdorff95		
	Whole	Core	Enhancing	Whole	Core	Enhancing
Abouelenien et al.[22]	0.852	0.812	0.741	8.25	**3.3**	**3.3**
Kermi et al.[23]	0.867	0.798	0.717	8.7	6.4	4.7
K. Hu et al.[24]	0.882	0.748	0.717	12.6	9.6	5.6
Baid et al. [25]	0.878	0.82	0.748	12.9	11	7.2
Frey et al.[26]	**0.896**	0.80	0.787	8.17	8.24	6.0
MIRAU-Net(our)	0.885	**0.879**	**0.818**	**7.02**	7.2	5.2

In the comparison presented in Table 3, MIRAU-Net exceeds other top entries in the core tumor and enhancing in the DSC value and is just less than the approach introduced by Frey et al. [26] on the whole tumor. Frey et al. [26] proposed a framework using a convolutional neural network. Compared

[4]https://www.cbica.upenn.edu/BraTS19/lboardTraining.html

with Abouelenien et al.[22] and Baid et al. [25] methods, our MIRAU-Net model achieves enhanced segmentation efficiency. K. Hu et al. [24] apply multi-cascaded convolutional neural networks. However, our MIRAU-Net achieved 0.3% on the whole tumor, 13.1% on the core tumor, and 10.1% enhancing tumor gains over [27]. In comparison with the proposed brain tumor segmentation network in [23], Our MIRAU-Net surpasses this network in the whole tumor, core tumor, and tumor enhancement by a large margin of 1.8%,8.1%, and 10.1%. By comparing the Hausdorff95 distance, our MIRAU-Net achieves the Hausdorff95 distance value of 7.00, 7.2, and 5.2, respectively, on the whole tumor, core tumor, and enhancing tumor segmentation. Mainly, it gains the optimal Hausdorff95 metric on complete tumor segmentation. However, the best distance value on core tumor and enhancing tumor are respectively obtained by Abouelenien et al. [22]. In general, Our MIRAU-Net model attains competitive performance and outperforms other state-of-the-art methodologies. The comparisons also indicate the effectiveness and the quality of our networks.

3.4.2. Evaluation Results on Brats 2019 Validation Dataset

We use 66 validation cases dataset for validation to take part in the Brats 2019 competition. The segmentation efficiency of our algorithm (MIRAU-Net) was calculated by using the online evaluation system for DSC and Hausdorff distance in the challenge leaderboard Web site[5]. Our results are available in the leaderboard section of these challenges under the title "Attention Inception Residual." The experimental results are shown in Table 4. Quantitatively, Dice scores are 0.866, 0.858, and 0.808 for the whole tumor, core tumor, and enhancing tumor, respectively. The table also displays the mean, standard deviation, median, and 25th and 75th percentile of each metric. Table 5 demonstrates comparative results with other traditional approaches.

MIRAU-Net achieves very competitive efficiency relative to other state-of-the-art brain tumor segmentation approaches. MIRAU-Net achieves DSC values

[5]https://www.cbica.upenn.edu/BraTS19/lboardValidation.html

Table 4: Evaluation results on Brats 2019 Validation Dataset

	Dice			Hausdorff distance		
	Whole	Core	Enhancing	Whole	Core	Enhancing
Mean	0.866	0.858	0.808	9.5	11.2	8.01
Std.Dev.	0.108	0.130	0.144	17.8	19.5	18.8
Median	0.90	0.901	0.85	4.1	4.3	2.3
25 quantile	0.86	0.858	0.78	3	2.05	1.4
75quantile	0.928	0.934	0.89	5.9	8.8	3.9

Table 5: Compared segmentation results with typical methods on Brats 2019 validation Dataset.

Methods	DSC			Hausdorff95		
	Whole	Core	Enhancing	Whole	Core	Enhancing
Chen et al.[28]	**0.894**	0.831	0.749	-	-	-
Islam et al.[29]	0.876	0.761	0.689	9.8	12.36	12.94
Hu et al.[30]	0.81	0.69	0.55	24.2	31.5	64.4
Chandra et al. [31]	0.83	0.73	0.618	20.45	26.48	24.93
Li et al.[32]	0.89	0.733	0.726	-	-	-
Baid et al. .[25]	0.878	0.826	0.748	12.9	**11.2**	**7.3**
MIRAU-Net(our)	0.866	**0.858**	**0.808**	**9.5**	**11.2**	8.01

of 86.6%, 85.8%, and 80.8% on the whole tumor, core tumor, and enhancing tumor, respectively. Specifically, our approach achieves the best values DSC of the core tumor, enhancing tumor and Hausdorff95 of the whole tumor region. The method proposed by Chen et al. [28] achieved slightly higher on complete tumor segmentation. Their approach proposed separable 3D U-Net architecture, but their models cannot achieve good segmentation results for each view. Our MIRAU-Net achieves better segmentation performance on DSC and Hausdorff95 compared with some recent approaches by Islam et al. [29] and Hu et al .[30].

Fig 5 shows the results of three HGG tumor samples and five LGG tumor

Table 6: Compared segmentation results with baselines on BraTS 2019 Validation Dataset

Methods	Whole	Core	Enhancing
U-Net	0.864	0.746	0.694
AGU-Net(our)	0.865	0.83	0.79
MIRAU-Net (our)	**0.866**	**0.858**	**0.808**

samples. In these figures, columns one to three display Flair, ground truth, and our MIRAU-Net segmentation, respectively. Where intratumor areas can be distinguished by color code: yellow for enhancing tumor, green for edema and necrotic, and red for non-enhancing. Fig. 5 indicates that the size, shape, location, and intensity of tumors in these eight samples are different and enhance the segmentation performance for small tumor regions. Generally, the proposed segmentation architecture results are comparable to those acquired by the experts (GT). Figure.6 shows the results for Dice and Hausdorff in validation data. The boxplots show the minimum, median, maximum, lower, and upper quartile. Points outside of the interquartile are referred to as outliers. From the boxplots, it was evident that our algorithm achieves considerably high segmentation accuracy in most cases. Fig. 7 Represents bar plots of the average DSC scores for the BraTS 2019 validation dataset for the three tumor regions. In this experiment, MIRAU-Net achieves superior segmentation efficiency in the three tumor regions relative to its baseline U-Net. In Table 6, MIRAU-Net achieves superior segmentation performance than its baseline U-Net for the three tumor regions. Meanwhile, AGU-Net outperforms U-Net by 0.1%for whole tumor, 8.4% for core tumor, and 9.6% for enhancing tumor respectively. Which is due to the effectiveness of multi Inception-residual with attention gates in improving brain tumor segmentation. Also Table .6 shows an increase in both Dice scores and Hausdorff95 distances the improvements due to the use of multi loss functions.

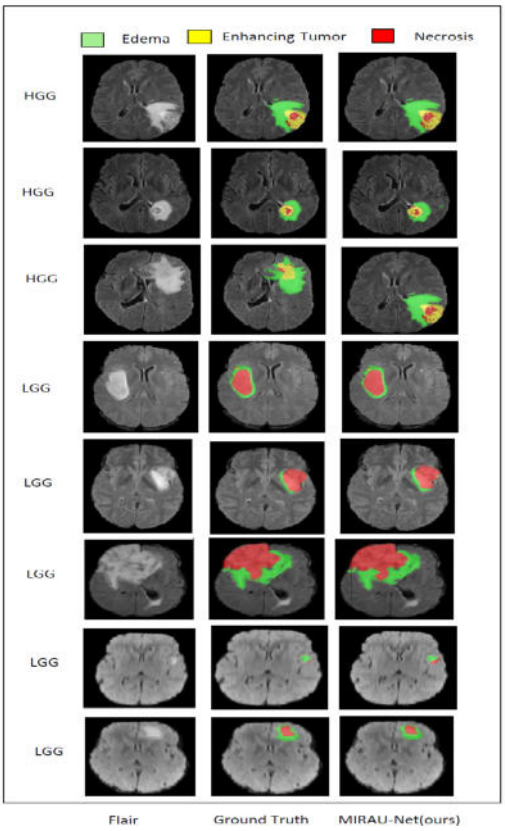

Figure 5: Samples of results of the BraTS 2019 training dataset segmentation. Flair image, Ground Truth, and MIRAU-Net respectively from left to right. Each color describes the class of tumor: red—necrosis and non-enhancing, green—edema, and yellow—enhancing tumor.

4. Conclusion

In this article, we suggested a new MIRAU-Net model for an automated method for brain tumor segmentation. First, we embedded the residual inception module and attention gate into U-Net in each block to enhance brain tumor segmentation performance. Then sub-networks encoder and decoder with connected by multi-inception residual pathways. A new multi-loss function is also introduced to reduce class imbalance by integrating the weight cross-entropy loss, Generalized Dice Loss, and Focal Tversky loss functions. The MIRAU-

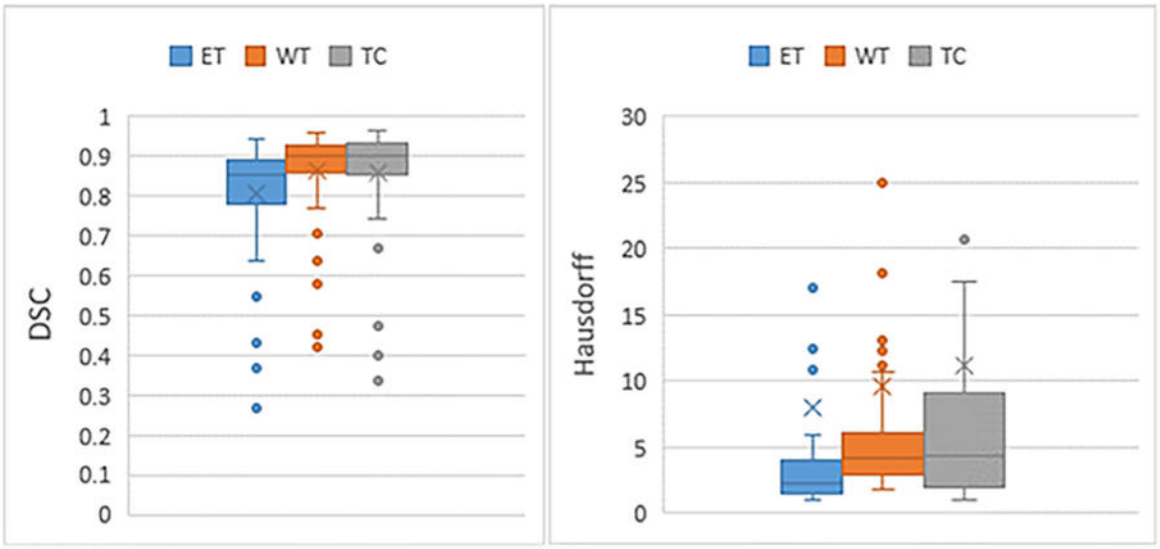

Figure 6: Boxplots of DSC and Hausdorff from validation data BraTS'2019. The 'x' signifies the mean score,"∘ " shows outliers.

Net architecture provides more excellent performance, especially for the segmentation of small-scale brain tumors. The suggested methodology was evaluated using the Brats'2019 dataset online. The experiment results showed that MIRAU-Net surpassed the U-Net and other typical brain tumor segmentation approaches by a large margin. So we will expand our MIRAU-Net in the future to 3D to improve segmentation performance. Besides, for further evaluation, we will extend our model to other medical segmentation image tasks.

Acknowledgment

This work was partially supported by National Funds through FCT/MCTES (Portuguese Foundation for Science and Technology), within the CISTER Research Unit (UIDP/UIDB/04234/2020).

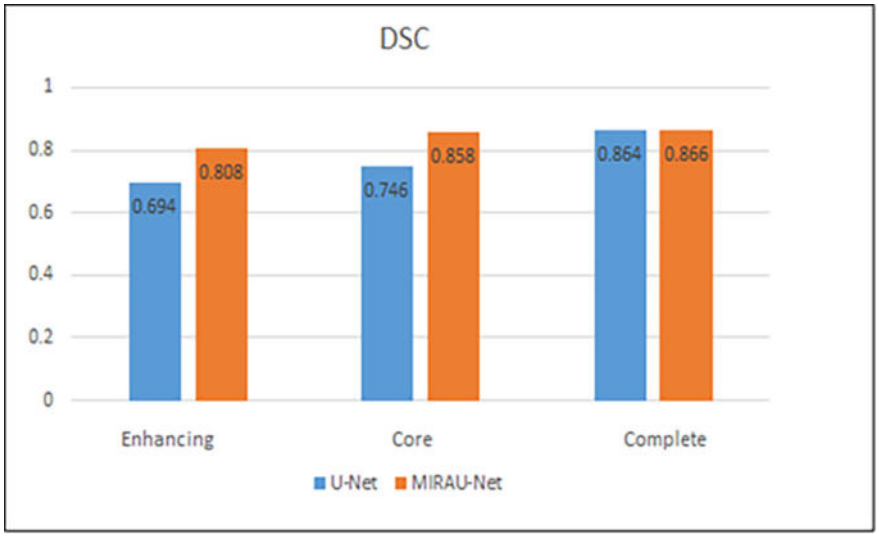

Figure 7: The DSC score Comparison for the BraTS 2019 validation dataset.

Table 7: Evaluation of different combinations of losses in MIRAU-Net, measured in terms of Dice scores and Hausdorff95 distances (mm)

Loss	Dice Score			Hausdorff95 distance		
	Whole	Core	Enhancing	Whole	Core	Enhancing
$L_{weightcrossentropy}$	0.80	0.828	0.857	9.6	11.9	9.7
$L_{weightcrossentropy}$+L_{GDL}	0.801	0.844	0.865	8.6	11.0	9.5
$L_{weightcrossentropy}$+L_{GDL}+$L_{FocalTverskyloss}$	0.808	0.858	0.866	8.01	11.2	9.5

References

[1] L.Yang, Y.Zhang, I.H.Guldner, S.Zhang, D.Z.Chen, 3d segmentation of glial cells using fully convolutional networks and k-terminal cut,in:International Conference on Medical Image Computing and Computer-Assisted Intervention,Springer,2016, pp. 658–666,doi:10.1007/978–3–319–46723–876

[2] X.Castells, J.M.García-Gómez, A. Navarro, J.J. Acebes, Automated brain tumor biopsy prediction using single-labeling cDNA microarrays-based gene expression profiling,Diagnostic Molecular Pathology 18 (4) (2009) 206–218.

[3] R.Girshick, J. Donahue, T.Darrell, J.Malik, Rich feature hierarchies for accurate object detection and semantic segmentation, in: Proceedings of the IEEE conference on computer vision and pattern recognition, 2014, pp.580–587.

[4] M.Havaei, A.Davy, D.Warde-Farley, A.Biard, Brain tumor segmentation with deep neural networks, Medical image analysis (2017) 18–31.

[5] H.Shen, R.Wang, J.Zhang, S.J. McKenna, Boundary-aware fully convolutional network for brain tumor segmentation, in: International Conference on Medical Image Computing and Computer-Assisted Intervention,Springer, 2017, pp. 433–441.

[6] O. Ronneberger, P. Fischer, T. Brox, U-net:Convolutional networks for biomedical image segmentation, in:International Conference on Medical image computing and computer-assisted intervention, Springer, 2015, pp.320234–241, doi: 10.1007/978–3–319–24574–428.

[7] K. He, X. Zhang, S. Ren, Deep residual learning for image recognition, in: Proceedings of the IEEE conference on computer vision and pattern recognition, 2016, pp. 770–778.

[8] M. Shaikh, G. Anand, G. Acharya, A. Amrutkar, Brain tumor segmentation using dense fully convolutional neural network, in: International MICCAI brainlesion workshop, Springer, 2017, pp. 309–319.

[9] D. E. Cahall, G. Rasool, N. C. Bouaynaya, H.M Fathallah-Shaykh, Inception modules enhance brain tumor segmentation, Frontiers in computational neuroscience 13 (2019) 44 , doi: 10.3389/fncom.2019.00044. eCollection 2019.

[10] F.Wang, M.Jiang, C.Qian, S. Yang, Residual attention network for image classification, in: Proceedings of the IEEE conference on computer vision and pattern recognition, 2017, pp. 3156–3164.

[11] J.Hu, L. Shen, G. Sun, Squeeze-and-excitation networks, in: Proceedings of the IEEE conference on computer vision and pattern recognition, 2018,pp. 7132–7141

[12] J. Zhang, Z. Jiang, J. Dong, Y. Hou, Attention Gate ResU-Net for automatic MRI brain tumor segmentation, IEEE Access 8 (2020) 58533–58545, doi:10.1109/ACCESS.2020.2983075.

[13] C. Szegedy, S.Ioffe, Inception-v4, inception-resnet and the impact of residual connections on learning, in:Proceedings of the AAAI Conference on Artificial Intelligence, Vol. 31, 2017, doi/10.5555/3298023.3298188.

[14] K. He, X. Zhang, S. Ren, Delving deep into rectifiers: Surpassing human-level performance on imagenet classification, in: Proceedings of the IEEE international conference on computer vision, 2015, pp.1026–1034.

[15] O.Oktay, J.Schlemper, L.L. Folgoc, et al., Attention u-net: Learning where to look for the pancreas, arXiv preprint arXiv:1804.03999.

[16] S. Lu, F. Gao, C. Piao, Dynamic weighted cross entropy for semantic segmentation with extremely imbalanced data, in: 2019 International Conference on Artificial Intelligence and Advanced Manufacturing (AIAM), IEEE,2019, pp.230–233.

[17] C.H.Sudre, W. Li, T.a. Vercauteren, Generalised dice overlap as a deep learning loss function for highly unbalanced segmentations, in: Deep learning in medical image analysis and multimodal learning for clinical decision support, Springer, 2017, pp. 240–248.

[18] S.Jadon, O.P. Leary, I. Pan, T.J.Harder, A comparative study of 2D image segmentation algorithms for traumatic brain lesions using CT data from the protectiii multicenter clinical trial, in: Medical Imaging 2020: Imaging Informatics for Healthcare, Research, and Applications, Vol. 11318, International Society for Optics and Photonics, 2020, p. 113180Q.

[19] A. TensorFlow, A System for Large-Scale Machine Learning This paper is included in the Proceedings of the TensorFlow: A system for large-scale machine learning, in: Proc 12th USENIX Conf. Oper. Syst. Des. Imple-
360 ment,2016.

[20] A.A.Taha, A.Hanbury, Metrics for evaluating 3D medical image segmentation: analysis, selection, and tool, BMC medical imaging 15 (1) (2015)1–28

[21] A.A.Taha, A.Hanbury, An efficient algorithm for calculating the exact Hausdorff distance, , IEEE transactions on pattern analysis and machine
365 intelligence 37 (11) (2015) 2153–2163.

[22] N.M.Aboelenein, P.Songhao, A.Koubaa, A. Noor, A. Afifi, HTTU-Net: Hybrid Two Track U-Net for automatic brain tumor segmentation, IEEE Access 8 (2020) 101406–101415.

[23] A.Kermi, I. Mahmoudi, M.T.Khadir, Deep convolutional neural networks
370 using U-Net for automatic brain tumor segmentation in multimodal MRI volumes, in: International MICCAI Brainlesion Workshop, Springer, 2018,pp. 37–48.

[24] K.Hu, Q.Gan, Y. Zhang, S.Deng, F. Xiao, W. Huang, C. Cao, X. Gao, Brain tumor segmentation using multi-cascaded convolutional neural net-
375 works and conditional random field, IEEE Access 7 (2019) 92615–92629.

[25] U.Baid, S. Talbar, S. Rane, S.Gupta, M.H.Thakur, A. Moiyadi, A novel approach for fully automatic intra-tumor segmentation with 3D U-Net architecture for gliomas, Frontiers in computational neuroscience 14 (2020) 10.

[26] M.Frey, M. Nau, Memory efficient brain tumor segmentation using an
380 autoencoder-regularized U-net, , in: International MICCAI Brainlesion Workshop, Springer, 2019, pp. 388–396.

[27] X.Zhao, Y.Wu, G. Song, A deep learning model integrating FCNNs and CRFs for brain tumor segmentation, Medical image analysis 43 (2018) 98–111.

[28] W.Chen, B.Liu, S. Peng, S3D-UNet: separable 3D U-Net for brain tumor segmentation, in: International MICCAI Brainlesion Workshop, Springer,2018, pp. 358–368.

[29] M.Islam, H. Ren, Multi-modal pixelnet for brain tumor segmentation, in: International MICCAI Brainlesion Workshop, Springer, 2017, pp. 298–308.

[30] Y. Hu, Y. Xia, 3D deep neural network-based brain tumor segmentation using multimodality magnetic resonance sequences,, in: International MICCAI Brainlesion Workshop, Springer, 2017, pp. 423–434.

[31] S.Chandra, M. Vakalopoulou, L. Fidon, Battistella, C. Robert, Context aware 3D CNNs for brain tumor segmentation, in: International MICCAI Brainlesion Workshop, Springer,2018, pp. 299–310.

[32] H.Li, A. Li, M.Wang, A novel end-to-end brain tumor segmentation method using improved fully convolutional networks, Computers in biology and medicine 108 (2019) 150–160.